

Smoothing and Adaptive Stretching of Discontinuous Fields in Finite Element Applications

MINVYDAS RAGULSKIS

Department of Mathematical Research in Systems
Kaunas University of Technology
Studentu 50-222, Kaunas LT-51368
LITHUANIA
<http://www.ktu.lt>

ALGIMANTAS FEDARAVICIUS

Department of Theoretical Mechanics
Kaunas University of Technology
Kestucio 27, Kaunas LT-44025
LITHUANIA
<http://www.ktu.lt>

JURATE RAGULSKIENE

Department of Technical Sciences
Kaunas College
Pramones 20, Kaunas LT-50468
LITHUANIA
<http://www.kauko.lt>

Abstract: - A technique for adaptive conjugate smoothing of discontinuous fields is presented in the paper. The described technique is applicable in various engineering problems and is especially effective when hybrid numerical – experimental methodologies are used. Adaptive image smoothing and stretching strategy is illustrated for a discontinuous plain stress field problem when photoelastic fringes representing the variation of stress are constructed in virtual projection plane.

Key-Words: - Discontinuous field, Smoothing, Finite element method, Interference fringes

1 Introduction

Visualisation techniques of the results from finite element analysis procedures are important due to several reasons. First is the meaningful and accurate representation of processes taking place in the analysed structures. Second, and perhaps even more important, is building the ground for hybrid numerical - experimental techniques. A typical example of finite element analysis in developing a hybrid technique is presented in [1].

Unfortunately, conventional FEM analysis techniques are based on the approximation of nodal displacements (not stresses) via the shape functions. Ramesh et al [2] have correctly noted that photoelastic isochromatics can be effectively used for the detection of FEM meshing problems.

Conventional FEM would require unacceptably dense meshing for producing sufficiently smooth

photoelastic patterns. Multiscale meshing is not affordable either - the whole domain of the structure must be analysed with the same accuracy. Therefore there exists a need for the development of a technique for smoothing the generated photoelastic fringe patterns representing the stress distribution and calculated from the displacement distribution. The proposed smoothing technique is based on conjugate approximation used for the calculation of nodal values of stresses and provides the digital images of acceptable quality on relatively rather coarse meshes.

The purpose of the paper is the development of techniques for smoothing of discontinuous fields applicable in finite element analysis enabling effective interpretation of experimental results what provides insight into the physical processes taking place in the analysed objects.

2 Smoothing of Discontinuous Fields

The components of stresses in the domain of the analysed finite element can be calculated in the usual way [3]:

$$\begin{Bmatrix} \sigma_x \\ \sigma_y \\ \tau_{xy} \end{Bmatrix} = [D][B]\{\delta_0\}, \quad (1)$$

where $\{\delta_0\}$ is the vector of nodal displacements of the eigenmode; $[B]$ is the matrix relating the strains with the displacements; $[D]$ is the matrix relating the stresses with the strains; $\sigma_x, \sigma_y, \tau_{xy}$ are the components of the stresses in the problem of plane stress. It can be noted that the displacements are continuous at interelement boundaries, but the calculated stresses are discontinuous due to the operation of differentiation.

The most natural way for the calculation of the nodal values of stresses is the minimisation of the squared difference between the discontinuous strain field defined by eq.(1) and the interpolated stress field through the nodal values of the stress components. That difference is integrated in the domains of the appropriate elements:

$$\sum_i \frac{1}{2} \iint_{e_i} ([N]\{\delta\} - \sigma)^2 dx dy, \quad (2)$$

where σ denotes corresponding component of stress; $\{\delta\}$ is the vector of nodal values of σ ; $[N]$ is the row of the shape functions of the finite element; e_i stands for the domain of the i -th finite element; summation denotes the direct stiffness procedure in the global domain [3].

Unfortunately, the solution of unknown nodal values $\{\delta\}$ from eq.(2) is unsatisfactory for generation of digital photoelastic images as the derivatives of the interpolated stress fields are still discontinuous. That is illustrated in the numerical results. Therefore, additional penalty terms for fast variation of the stress fields are introduced:

$$\lambda \left(\left(\frac{\partial \sigma}{\partial x} \right)^2 + \left(\frac{\partial \sigma}{\partial y} \right)^2 \right), \quad (3)$$

where λ is a parameter of smoothing. Addition of the penalty term defined in eq.(3) to the residual in eq.(2) after elementary transformations leads to:

$$\sum_i \frac{1}{2} \iint_{e_i} \left(([N]\{\delta\} - \sigma)^2 + \lambda \{\delta\}^T [C]^T [C] \{\delta\} \right) dx dy, \quad (4)$$

where $[C]$ is the matrix of the derivatives of the shape functions. The minimisation of residuals defined by eq.(4) leads to the following systems of linear algebraic equations for the determination of each of the component of the stresses:

$$\begin{aligned} & \left(\sum_i \iint_{e_i} ([N]^T [N] + [C]^T \lambda [C]) dx dy \right) \cdot \{\delta\} = \\ & = \sum_i \iint_{e_i} [N]^T \sigma dx dy \end{aligned} \quad (5)$$

The selection of the smoothing parameter λ can be performed using the error norms of the finite elements [3] and the components of the stresses are interpolated from their nodal values by using the shape functions of the finite elements.

3 One-Dimensional Example

The formulation of the smoothing procedure is illustrated by one-dimensional model comprising three finite elements each consisting from 3 nodes (Fig. 1). The co-ordinates of the nodes are $x_k = k - 1; k = 1, 2, \dots, 7$.

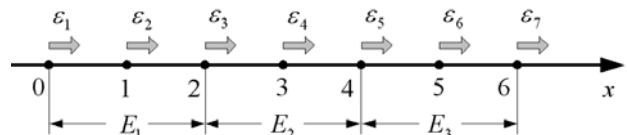


Fig. 1. One-dimensional example.

Then, the shape functions of the i -th finite element are:

$$\begin{aligned} N_1^{(i)}(x) &= 2i^2 - i + \left(\frac{1}{2} - 2i \right) \cdot x + \frac{1}{2} \cdot x^2; \\ N_2^{(i)}(x) &= 4i - 4i^2 + (4i - 2)x - x^2; \\ N_3^{(i)}(x) &= 2i^2 - 3i + 1 + \left(\frac{3}{2} - 2i \right) \cdot x + \frac{1}{2} \cdot x^2. \end{aligned} \quad (6)$$

The distribution of strain and stress fields in the domain of the i -th element is interpolated as:

$$\begin{aligned} \varepsilon^{(i)}(x) &= \\ &= N_1^{(i)}(x)\varepsilon_{2i-1} + N_2^{(i)}(x)\varepsilon_{2i} + N_3^{(i)}(x)\varepsilon_{2i+1}; \end{aligned}$$

$$\begin{aligned} \sigma^{(i)}(x) &= \\ &= B_1^{(i)}(x)\varepsilon_{2i-1} + B_2^{(i)}(x)\varepsilon_{2i} + B_3^{(i)}(x)\varepsilon_{2i+1}, \end{aligned} \quad (7)$$

where $B_j^{(i)}$ is the derivative of shape function $N_j^{(i)}$, $j=1, \dots, 3$. Then, elementary transformations lead to:

$$\begin{aligned} \int_{2(i-1)}^{2i} [N]^T [N] dx &= \begin{bmatrix} \frac{4}{15} & \frac{2}{15} & -\frac{1}{15} \\ \frac{2}{15} & \frac{16}{15} & \frac{2}{15} \\ -\frac{1}{15} & \frac{2}{15} & \frac{4}{15} \end{bmatrix}; \\ \int_{2(i-1)}^{2i} [C]^T [C] dx &= \begin{bmatrix} \frac{7}{6} & -\frac{4}{3} & \frac{1}{6} \\ -\frac{4}{3} & \frac{8}{3} & -\frac{4}{3} \\ \frac{1}{6} & -\frac{4}{3} & \frac{7}{6} \end{bmatrix}; \\ \int_{2(i-1)}^{2i} [N]^T \sigma^{(i)} dx &= \begin{bmatrix} -\frac{1}{2}\varepsilon_{2i-1} + \frac{2}{3}\varepsilon_{2i} - \frac{1}{6}\varepsilon_{2i+1} \\ -\frac{2}{3}\varepsilon_{2i-1} + \frac{2}{3}\varepsilon_{2i+1} \\ \frac{1}{6}\varepsilon_{2i-1} - \frac{2}{3}\varepsilon_{2i} + \frac{1}{2}\varepsilon_{2i+1} \end{bmatrix}. \end{aligned} \quad (8)$$

Summation over the global domain and solution of algebraic system of equations in eq. (5) produces a set of discrete nodal components of stress $\{\delta\}$ which can be interpolated in the domains of appropriate finite elements:

$$\begin{aligned} S^{(i)}(x, \lambda) &= \\ &= \delta_{2i-1}(\lambda)N_1^{(i)}(x) + \delta_{2i}(\lambda)N_2^{(i)}(x) + \delta_{2i+1}(\lambda)N_3^{(i)}(x). \end{aligned} \quad (9)$$

Particularly, for $\varepsilon_1=0.4$; $\varepsilon_2=0.35$; $\varepsilon_3=0.2$; $\varepsilon_4=0.4$; $\varepsilon_5=0.53$; $\varepsilon_6=0.55$ and $\varepsilon_7=0.8$ the theoretical discontinuous, interpolated continuous and smoothed continuous fields of stresses are presented in Fig. 2. Array of thin solid lines correspond to increasing values of the smoothing parameter λ .

It can be noted, that the smoothed fields of stresses is much more compressed comparing with the theoretical discontinuous field of stresses. Therefore the number of reconstructed interference fringes would be too small and would not represent the physical effects taking place in the analysed system. This problem can be avoided by stretching the smoothed field of stresses to the limits of the non-smoothed field.

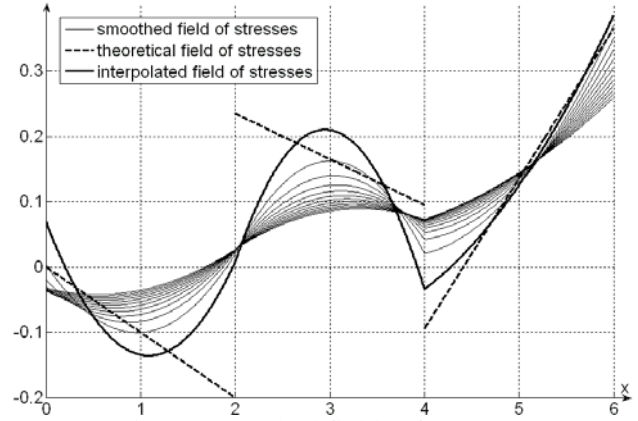


Fig. 2. Smoothed fields of stresses.

Explicitly,

$$I^* = \frac{M_0 - m_0}{M_a - m_a} \cdot I_a + \frac{m_0 M_a - m_a M_0}{M_a - m_a}, \quad (10)$$

where I_a is the smoothed field; I^* is the stretched field;

$$\begin{aligned} m_0 &= \inf_i \left(\min_x S^{(i)}(x, 0) \right); \\ M_0 &= \sup_i \left(\max_x S^{(i)}(x, 0) \right); \\ m_a &= \inf_i \left(\min_x S^{(i)}(x, \lambda \cdot R) \right); \\ M_a &= \sup_i \left(\max_x S^{(i)}(x, \lambda \cdot R) \right). \end{aligned} \quad (11)$$

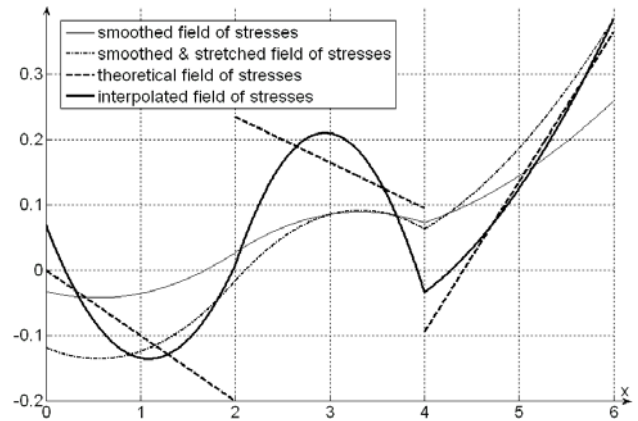


Fig. 3. Smoothed and stretched fields of stresses.

Fig. 3 presents the effect of stretching when the field of stress is not only smoothed but also stretched up to range of numerical values which guarantees correct representation of stress distribution in the global domain.

3 Finite Element Model

The problem of smoothing of discontinuous fields is illustrated by finite element analysis of bending

vibrations of micromechanical components comprising photoelastic coatings. Bending vibrations are common in different engineering and physical applications. Bending vibrations of centrally clamped rotating circular disks play crucial role in the functionality of hard disk drives. Lots of efforts are spent for dynamic stabilisation, control and measurement of bending vibrations in such micro-mechanical systems [4].

Measurement of microscopic deflections from the state of equilibrium is a challenging experimental problem. Different optical measurement techniques are developed for experimental investigation of bending vibrations [5]. Unfortunately, interpretation of experimental measurement results is a nontrivial inverse engineering problem often having non-unique solutions. Therefore there exists a definite need for hybrid numerical – experimental techniques that could help to interpret the measurement results (Fig. 3).

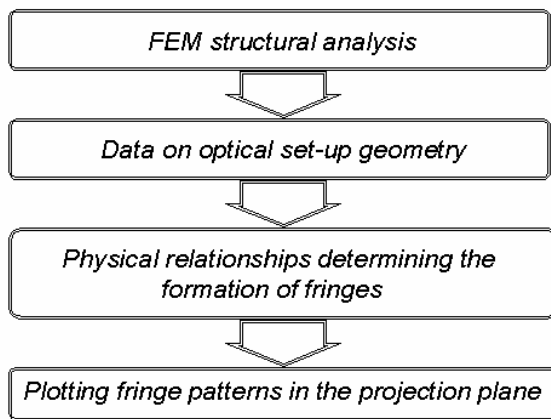


Fig. 3. Schematic diagram of hybrid numerical-experimental techniques.

Such techniques usually comprise a numerical model of the system coupled with optical and geometrical parameters of the measurement set-up. Then the predicted response of the experimental optical measurement system can be mimicked in virtual numerical environment when the dynamical parameters of the analysed object are pre-defined.

Finite element mesh of a vibrating micromechanical centrally clamped disk is shown in Fig. 4. The mesh in the status of equilibrium is grey and deflected according to the eigenmode is black. Finite element techniques are used to construct the numerical model of a centrally clamped circular disk.

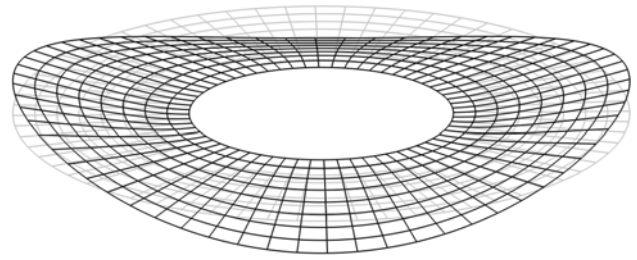


Fig. 4. Finite element mesh of disk with clamped internal radius.

Plate bending element with the independent interpolation of the displacement w and the rotations about the appropriate axes θ_x and θ_y is used [3]. The schematic representation of the plate and the coating is shown in Fig. 1. x , y and z are the axes of the orthogonal Cartesian system of coordinates; w is the displacement of the plate; θ_x and θ_y are the rotations of the plate about the appropriate axes; $u = \frac{h}{2}\theta_y$,

and $v = -\frac{h}{2}\theta_x$ are the displacements on the surface of the plate; h is the thickness of the plate; d is the thickness of the photo-elastic coating.

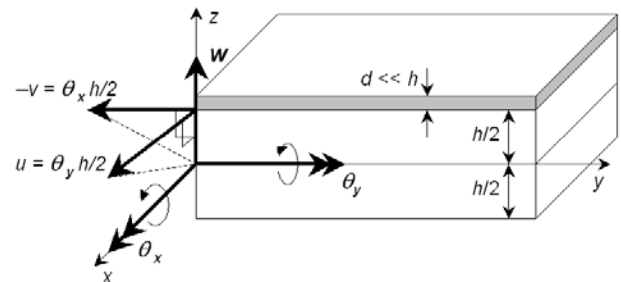


Fig. 4. Schematic model of the finite element.

The nodal variables of the plate bending element are the deflection of the plate w , the rotation of the plate about the x axis θ_x and the rotation of the plate about the y axis θ_y .

The principal stresses σ_1 , σ_2 at each node are calculated as the eigenvalues of the matrix:

$$\begin{bmatrix} \sigma_x & \tau_{xy} \\ \tau_{xy} & \sigma_y \end{bmatrix}, \quad (12)$$

and the normalised eigenvectors of this matrix $\{V_1\}$, $\{V_2\}$ are the directions of the principal stresses. The vector of polarisation is given as:

$$\{P\} = \begin{Bmatrix} \cos \alpha \\ \sin \alpha \end{Bmatrix}, \quad (13)$$

where α is the angle of the vector of polarisation. Then the intensity in the photoelastic image of the plane polariscope (isoclinics and isochromatics intertwined) is calculated as

$$I = ((\{V_1\} \cdot \{P\})(\{V_2\} \cdot \{P\}) \sin C(\sigma_1 - \sigma_2))^2, \quad (14)$$

where C is the constant dependent on the thickness of the analysed structure in the state of plane stress and on the material from which it is produced. The intensity of the photoelastic image for the circular polariscope (isochromatics) is calculated as:

$$I = (\sin C(\sigma_1 - \sigma_2))^2. \quad (15)$$

The relationships presented above form the basis for the generation of digital photoelastic images. The procedure of construction of digital images in projection planes from isoparametric finite elements is described in detail in [6].

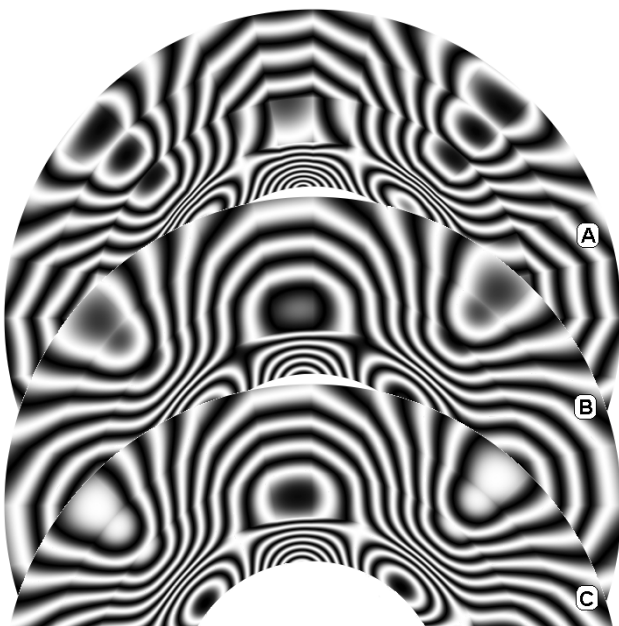


Fig. 5. Photoelastic images of a clamped disk: A – unsmoothed image; B – smoothed image; C – smoothed and stretched image

Photoelastic fringes (circular isochromatics) of the vibrating disk are presented in Fig. 5. Three images are overlapped due to the space limitations. It can be clearly seen that the fringes are broken in the unsmoothed image A, what is unacceptable for stress field analysis. The smoothing procedure produces better pattern of fringes (Fig. 5.B). Nevertheless, it can be notes that the number of fringes in the smoothed image is less that in the original unsmoothed one. Stretching of the field of

stresses up to the original range of values (Fig. 5.C) provides correct number of fringes with acceptable smoothness.



Fig. 6. Isoclinics and isochromatics intertwined.

Finally, isoclinics and isochromatics intertwined are presented in Fig. 6 (polarization angle $\alpha = \pi/8$). Such numerical reconstruction provides high quality digital images well acceptable for hybrid numerical – experimental techniques.

4 Concluding Remarks

The displacement based FEM formulations are coupled with stress based photoelasticity analysis. As the stress field is discontinuous in the inter-element boundaries, the introduced smoothing and stretching procedure enables the generation of high quality digital images acceptable for hybrid numerical – experimental techniques.

It can be noted that the generation of the digital photoelastic images is not a straightforward procedure. It involved such steps as the construction of the numerical model of the analysed object; finite element calculations based on the loading scheme, boundary conditions; determination of the nodal vales of stress components and their smoothing; generation of appropriate digital images.

References:

- [1] A. Holstein, L. Salbut, M. Kujawinska, W. Juptner, Hybrid experimental-numerical concept of residual stress analysis in laser

- weldments, *Experimental Mechanics*, Vol.41, No.4, 2001, pp. 343-350.
- [2] K. Ramesh, P.M. Pathak, Role of photoelasticity in evolving discretization schemes for FE analysis, *Experimental Techniques*, Vol.23, No.4, 1999, pp. 36-38.
- [3] K.H. Huebner, D.L. Dewhirst, D.E. Smith, T.G. Byrom, *Finite element method*, Wiley, 2001.
- [4] P. Manzione, A.H. Nayfeh, Instability mechanisms of a centrally clamped rotating circular disk under a space-fixed spring-mass-dashpot system, *Journal of Vibration and Control*, Vol.7, No.7, 2001, pp. 1013-1034.
- [5] A.S. Kobayashi, *Handbook on experimental mechanics*, 2nd ed. SEM, 1993.
- [6] M. Ragulskis, A. Palevicius, L. Ragulskis, Plotting holographic interferograms for visualisation of dynamic results from finite element calculations, *International Journal for Numerical Methods in Engineering*, Vol.56, No.11, 2003, pp. 1647-1659.